Raman scattering near a *d*-wave Pomeranchuk instability

Hiroyuki Yamase[1] and Roland Zeyher[2]
[1]*National Institute for Materials Science, Tsukuba 305-0047, Japan*
[2]*Max-Planck-Institute for Solid State Research, Heisenbergstrasse 1, D-70569 Stuttgart, Germany*
(Received 30 September 2010; published 11 March 2011)

Motivated by recent transport and neutron-scattering experiments suggesting an orientational symmetry breaking in underdoped cuprates we present a theoretical study of Raman scattering near a *d*-wave Pomeranchuk instability (PI). The *d*-wave component of Raman scattering from electrons and phonons allows one to study directly order parameter fluctuations associated with the PI. Approaching the PI from the normal state by lowering the temperature, a central peak emerges both in electronic and, as an additional low-frequency feature, in phononic scattering. Approaching the PI in the superconducting state at low temperature by decreasing the doping concentration the central peak is replaced by a soft mode with strongly decreasing width and energy and increasing spectral weight. These predicted low-energy features in Raman scattering could confirm in a rather direct way the presence of a PI in high-temperature cuprate superconductors and in $Sr_3Ru_2O_7$.

DOI: 10.1103/PhysRevB.83.115116 PACS number(s): 74.25.nd, 74.25.Kc, 71.18.+y, 74.72.−h

I. INTRODUCTION

In condensed matter, electrons move through a crystal lattice whose symmetry is characterized by a point group. The electronic band structure usually has the same symmetry as the lattice and so does the Fermi surface. However, it was shown that the symmetry of the Fermi surface can be broken spontaneously by electron-electron correlations in the two-dimensional t-J (Refs. 1–3) and Hubbard[4,5] models leading to spontaneous Fermi-surface deformations characterized by a *d*-wave symmetry [*d*-wave Fermi-surface deformations (*d*FSD)]. This instability is frequently referred to as a *d*-wave Pomeranchuk instability, which is characterized by the violation of the stability criteria for isotropic Fermi liquids derived by Pomeranchuk.[6] However, it should be noted that the *d*FSD state can also be realized not only in strongly correlated electron systems such as those described by the t-J model[1–3] but also without a breaking of Pomeranchuk's stability criterion in systems where the transition can become of first order at low temperatures.[7,8] The *d*FSD state breaks only the orientational symmetry, that is, its instability is driven by zero momentum charge-density fluctuations with internal *d*-wave symmetry and leads to an electronic nematic state. As originally introduced in Ref. 9, an electronic nematic state can also be realized by invoking charge stripes. In a first step both orientational and translational symmetry are broken by condensing the electrons into a charge stripe state characterized by a set of large wave vectors which break the orientational symmetry. In a second step the stripes melt restoring the translational but not the orientational symmetry. In the following we restrict ourselves to the case where the *d*FSD leads directly to an electronic nematic state without first showing an instability toward stripes.

The double-layer strontium ruthenate $Sr_3Ru_2O_7$ (Sr327) has attracted much attention as a compound likely exhibiting a *d*FSD instability.[10–12] Compelling, but indirect, evidence for this comes from the observation of a strong xy anisotropy of the resistivity which is present only in the ordered phase.[11] Angle-resolved photoemission spectroscopy[13] (ARPES) and de Hass-van Alphen[14–16] measurements could detect Fermi-surface deformations directly, but convincing experimental evidence for their existence has not been obtained yet. Theoretically, many properties have been successfully interpreted in terms of a *d*FSD instability, for instance, the metamagnetic transition,[17] the enhancement of the residual resistivity,[18] the phase diagram and various thermodynamic quantities,[19] universal numbers,[20] the bilayer effect,[21,22] suppression of a critical temperature due to impurities,[23] the spin-orbit effect,[24] and orbital degree of freedom.[25] Theoretical predictions based on the *d*FSD instability were also made for the pattern of Friedel oscillation around an impurity,[26] the attenuation of ultrasound waves,[27] and the singular behavior of the uniform magnetic susceptibility at the *d*FSD instability.[28] A somewhat different scenario invoking orbital order has recently been proposed[29,30] to account for the anomalies in Sr327.

In the case of the high-temperature superconductors $YBa_2Cu_3O_y$ ($YBCO_y$), the dynamical in-plane magnetic susceptibility is strongly anisotropic, both for slightly underdoped [$YBCO_{6.6}$ (Refs. 31 and 32)] and optimally doped [$YBCO_{6.85}$ (Ref. 31)] compounds. The anisotropy increases with decreasing doping and is most pronounced around the onset temperature of superconductivity or of the pseudogap, whereas it is suppressed in the superconducting state. It was shown theoretically that these features can be well understood in terms of the competition of the singlet pairing formation and *d*FSD correlations.[33] In the strongly underdoped region ($YBCO_{6.45}$) neutron-scattering experiments revealed a qualitatively different feature of the anisotropy.[34] The in-plane anisotropy of the magnetic excitation spectrum increases monotonically below 150 K, saturates below 50 K, but is not suppressed below $T_c = 35$ K. Moreover, the low-energy spectral weight does not decrease below T_c but is rather enhanced. These peculiar phenomena can be interpreted as (i) a quantum phase transition to the *d*FSD state deep inside the superconducting state[35,36] or (ii) a substantial suppression of singlet pairing due to the competition with increasing *d*FSD correlations in the strongly underdoped region.[37]

Quite recently the measurement of the Nernst coefficient in the doping region from 11–18% in YBCO (Ref. 38) showed a strong xy anisotropy. It sets in near the temperature where the pseudogap appears so that the pseudogap region is interpreted as the region with a finite *d*FSD in agreement with

a theoretical study.[39] However, one should note that the regions where the in-plane anisotropy has been observed by neutron scattering[31,32,34] and by transport[38] differ from each other so that it is difficult at present to reach clear-cut conclusions. The experimental evidence for nematic order in cuprates has recently been critically reviewed in Ref. 40.

Usually an emergent instability can be studied by measuring the enhancement of the corresponding susceptibility. The susceptibility describing the dFSD is the d-wave charge compressibility,[1,4,8] which can be measured directly by Raman scattering. Hence Raman scattering can provide decisive evidence for a dFSD instability and its correlations in actual systems. However, despite various experimental studies in Sr327 and YBCO, Raman-scattering experiments have not been reported to confirm a dFSD in those materials.

In this paper we provide theoretical predictions of the Raman-scattering intensity from electrons and phonons near the dFSD instability in both normal and superconducting states by employing parameters appropriate to cuprate superconductors. In the superconducting state the Raman-scattering intensity can be computed in terms of the noninteracting electron propagator, i.e., without considering the damping of electrons. In the normal state, however, it is crucially important to include the electronic self-energy. We therefore include the Fock diagram for the self-energy, express it in terms of the bosonic spectral function $\alpha^2F(\omega)$, and fit the latter to the self-energy measured in ARPES.[41,42]

The paper is structured as follows. In Sec. II we present formulas for electronic and phononic Raman scattering near a dFSD instability. Since the order parameter for dFSD fluctuations has B_{1g} symmetry for a square lattice only the B_{1g} component of the Raman tensor and B_{1g} phonons will be directly affected by order-parameter fluctuations. In Sec. III we study Raman scattering for two different ways to approach the dFSD instability. In the first case the system is always in the normal state and the temperature is lowered for a fixed doping in the underdoped region. In the second case we assume that at low temperature the dFSD instability lies in the superconducting state and is reached by decreasing the doping. Results for both cases are given in this section. Section IV contains a detailed discussion of these results and our conclusions.

II. FORMALISM

In the following we will consider fermions on a square lattice which has the tetragonal point-group symmetry D_{4h}. Since the order parameter of the dFSD is the charge density with internal d-wave symmetry and zero total momentum, dFSD fluctuations will be most easily detected in the B_{1g} component of Raman scattering and for a zone-center phonon with B_{1g} symmetry. We therefore will focus on these two quantities in the following. Throughout the paper we will also use the lattice constant of the square lattice as the length unit.

A. Electronic Raman scattering

The electronic contribution to the B_{1g} Raman vertex is given in the effective mass approximation[43]

$$\gamma_{\mathbf{k}}^{B_{1g}} = \frac{1}{2}\left(\frac{\partial^2\epsilon_{\mathbf{k}}}{\partial k_x^2} - \frac{\partial^2\epsilon_{\mathbf{k}}}{\partial k_y^2}\right), \tag{1}$$

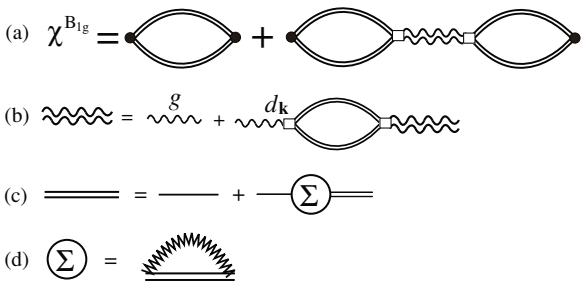

FIG. 1. (a) Graphical representation of $\chi^{B_{1g}}$. The vertex with a circle (square) indicates the form factor $\gamma_{\mathbf{k}}^{B_{1g}}$ ($d_{\mathbf{k}}$). (b) Effective electron-electron interaction driving the dFSD instability. (c) Full electronic Green's function. The single solid line denotes the free-electron propagator with the dispersion $\epsilon_{\mathbf{k}}$. (d) Electronic self-energy originating from the coupling to some bosonic fluctuations represented by the sawlike line.

where $\epsilon_{\mathbf{k}}$ is the electronic dispersion,

$$\epsilon_{\mathbf{k}} = -2t(\cos k_x + \cos k_y) - 4t' \cos k_x \cos k_y - 2t''(\cos 2k_x + \cos 2k_y), \tag{2}$$

with t, t', and t'' being the nearest-, second-nearest-, and third-nearest-neighbor hopping integrals, respectively. Inserting Eq. (2) into Eq. (1) yields

$$\gamma_{\mathbf{k}}^{B_{1g}} = t(\cos k_x - \cos k_y)[1 + 8t''(\cos k_x + \cos k_y)/t]. \tag{3}$$

The Raman-scattering intensity $S(\omega)$ is given by

$$S(\omega) = -\frac{1}{\pi}[1 + b(\omega)]\mathrm{Im}\,\chi^{B_{1g}}(\omega), \tag{4}$$

where $b(\omega)$ is the Bose function given by $(e^{\beta\omega} - 1)^{-1}$ and $\beta^{-1} = T$ is the temperature. The quantity $\chi^{B_{1g}}(\omega)$ is the retarded Green's function with two Raman vertices as end points and is given by

$$\chi^{B_{1g}}(\omega) = -\frac{i}{N}\int_0^\infty dt\, e^{i(\omega + i0^+)t}\langle[\rho_d(t), \rho_d(0)]\rangle, \tag{5}$$

where N is the total number of lattice sites, 0^+ is an infinitesimally small quantity, $\langle\cdots\rangle$ denotes the equilibrium expectation value, $[\cdot,\cdot]$ is the commutator, and $\rho_d(t)$ is the Heisenberg representation of the d-wave charge-density operator

$$\rho_d = \sum_{\mathbf{k},\sigma} \gamma_{\mathbf{k}}^{B_{1g}} c_{\mathbf{k}\sigma}^\dagger c_{\mathbf{k}\sigma} \tag{6}$$

with $c_{\mathbf{k}\sigma}^\dagger$ ($c_{\mathbf{k}\sigma}$) being the creation (annihilation) operator of electrons with spin σ and momentum $\mathbf{k}$. Within the random-phase approximation (RPA) $\chi^{B_{1g}}(\omega)$ is given by the bubble diagrams shown in Figs. 1(a) and 1(b). The double line represents the electronic Green's function. In the normal state, which we discuss first, self-energy corrections in the electronic Green's functions must be taken into account, as shown diagrammatically in Fig. 1(c). Otherwise each bubble would become zero in the zero-momentum limit at every finite frequency. This means that mainly the incoherent part of the Green's function contributes to Raman scattering in the normal state.

In order to get a finite self-energy we consider the coupling of electrons to some bosonic fluctuations, described by the Fock diagram shown in Fig. 1(d). Analytically one

obtains, adopting the usual approximations in evaluating the Eliashberg equations,[44]

$$\mathrm{Im}\,\Sigma(\omega) = -\pi\int_0^\infty d\nu\,\alpha^2F(\nu)[2b(\nu)+f(\nu-\omega)+f(\nu+\omega)], \quad (7)$$

where $f(\nu)=(e^{\beta\nu}+1)^{-1}$ is the Fermi function, and $\alpha^2F(\nu)$ specifies the bosonic spectral function. We have neglected the momentum dependence of α^2F for simplicity. Note that although the notation of $\alpha^2F(\nu)$ is often used in the context of a phonon spectrum, the bosonic modes in Fig. 1(d) are arbitrary in our model. We model the function $\alpha^2F(\nu)$ with three parameters, a_0, ν_0, and ν_c, as illustrated in Fig. 2(a). Comparing with ARPES measurements in the normal state in cuprates[41,42] we choose $\nu_0=\nu_c/4$, $\nu_c=2t/3$, and $a_0=1/4$ with $t\approx 150$ meV. In Fig. 2(b) we show $\mathrm{Im}\,\Sigma(\omega)$ for several choices of T. The magnitude of $\mathrm{Im}\,\Sigma(\omega)$ becomes larger with increasing T, indicating reductions of the lifetime of quasiparticles at higher T. As a function of energy, on the other hand, the longest lifetime of quasiparticle is realized on the Fermi surface, namely, at $\omega=0$; the magnitude of $\mathrm{Im}\,\Sigma(\omega)$ is enhanced with increasing ω and saturates to the value, $-\pi\int_0^\infty d\nu\,\alpha^2F(\nu)[2b(\nu)+1]$ for $\omega\to\infty$. The real part of $\Sigma(\omega)$ is computed numerically from the Kramers-Kronig relation, $\mathrm{Re}\,\Sigma(\omega)=\frac{1}{\pi}\,\mathrm{p.v.}\int_{-\infty}^{\infty}d\nu\frac{\mathrm{Im}\,\Sigma(\nu)}{\nu-\omega}$, where the integral is defined as the principal value denoted by "p.v." The obtained $\mathrm{Re}\,\Sigma(\omega)$ is shown in Fig. 2(c). The real part of $\Sigma(\omega)$ vanishes at $\omega=0$. Its magnitude forms a peak around $\omega\approx 0.5t$ and is suppressed at high ω with a tail characterized by ω^{-1}. Our self-energy reproduces well the data[41,42] extracted from ARPES measurements in cuprate superconductors.

The spectral function of the full Green's function [Fig. 1(c)] is given by

$$A(\mathbf{k},\omega) = -\frac{1}{\pi}\mathrm{Im}\,G(\mathbf{k},\omega) \quad (8)$$

$$= -\frac{1}{\pi}\frac{\mathrm{Im}\,\Sigma(\omega)}{[\omega-(\epsilon_{\mathbf{k}}-\mu)-\mathrm{Re}\,\Sigma(\omega)]^2+[\mathrm{Im}\,\Sigma(\omega)]^2}. \quad (9)$$

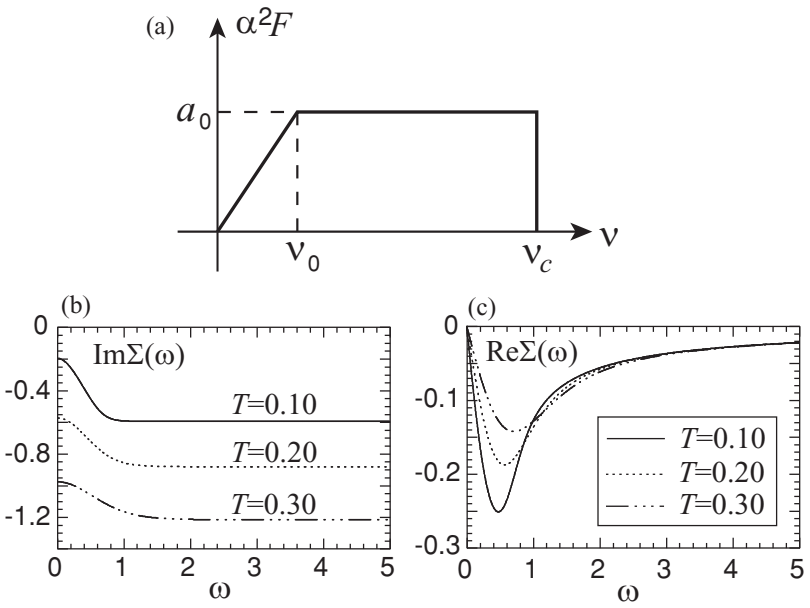

FIG. 2. (a) Model of $\alpha^2F(\nu)$. (b) Imaginary part and (c) real part of the electronic self-energy for several choices of T in the normal state for $\nu_0=\nu_c/4$, $\nu_c=2/3$, and $a_0=1/4$. The energy unit is taken as t.

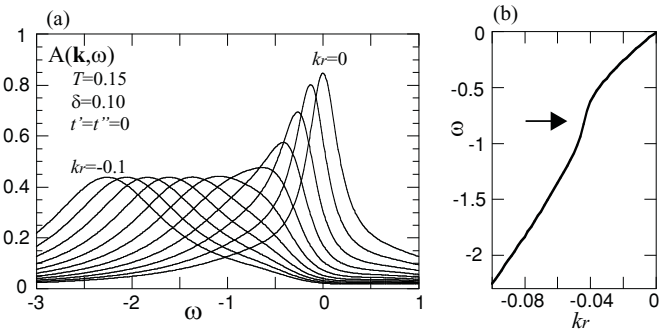

FIG. 3. (a) $A(\mathbf{k},\omega)$ as a function of ω at the momentum $\mathbf{k}-\mathbf{k}_F=2\pi k_r(1,1)$ with k_r ranging from zero to -0.10 with an interval of 0.01; $\mathbf{k}_F$ is the Fermi momentum along the $(0,0)-(\pi,\pi)$ direction. (b) The renormalized electronic dispersion.

Here μ is the chemical potential which is approximately determined by the relation $\delta=1-\frac{2}{N}\sum_{\mathbf{k}}f(\epsilon_{\mathbf{k}}-\mu)$ for a given doping concentration δ and T. Figure 3(a) shows $A(\mathbf{k},\omega)$ as a function of ω for several momenta along the $(0,0)-(\pi,\pi)$ direction. A relatively sharp peak is seen only close to the Fermi energy ($\omega=0$); away from the Fermi surface it is substantially broadened because of the presence of the sizable $\mathrm{Im}\,\Sigma(\omega)$. The peak position of $A(\mathbf{k},\omega)$ is plotted in Fig. 3(b). The renormalized electronic band dispersion displays a kink, as indicated by an arrow, due to the coupling to the bosonic fluctuations [Fig. 1(d)]. These features in Fig. 3 are qualitatively consistent with ARPES data.[41,42]

A single bubble diagram in Fig. 1(a) corresponds to the analytical expression,

$$\Pi^{\alpha\beta}(\omega)=\frac{2}{N}\sum_{\mathbf{k}}\alpha_{\mathbf{k}}\beta_{\mathbf{k}}\int_{-\infty}^{\infty}d\epsilon_1\,d\epsilon_2\,A(\mathbf{k},\epsilon_1)A(\mathbf{k},\epsilon_2)\times\frac{f(\epsilon_1)-f(\epsilon_2)}{\epsilon_1+\omega-\epsilon_2+i0^+}, \quad (10)$$

where the form factors of the vertices are denoted by $\alpha_{\mathbf{k}}$ and $\beta_{\mathbf{k}}$, which stand either for $\gamma_{\mathbf{k}}^{B_{1g}}$ [Eq. (3)] or $d_{\mathbf{k}}=\cos k_x-\cos k_y$.

For the imaginary part $\mathrm{Im}\,\Pi^{\alpha\beta}(\omega)$ we obtain

$$\mathrm{Im}\,\Pi^{\alpha\beta}(\omega) = \frac{2\pi}{N}\sum_{\mathbf{k}}\alpha_{\mathbf{k}}\beta_{\mathbf{k}}\int_{-\infty}^{\infty} d\epsilon\, A(\mathbf{k},\epsilon)A(\mathbf{k},\epsilon+\omega) \times [f(\epsilon+\omega)-f(\epsilon)]. \quad (11)$$

The real part $\mathrm{Re}\,\Pi^{\alpha\beta}(\omega)$ is determined from the Kramers-Kronig relation

$$\mathrm{Re}\,\Pi^{\alpha\beta}(\omega) = \frac{1}{\pi}\,\mathrm{p.v.}\int_{-\infty}^{\infty} d\nu \frac{\mathrm{Im}\,\Pi^{\alpha\beta}(\nu)}{\nu-\omega}. \quad (12)$$

Finally, the Raman response function $\chi^{B_{1g}}(\omega)$, described in Fig. 1(a), is given by

$$\chi^{B_{1g}}(\omega) = \Pi^{\gamma\gamma}(\omega) + \Pi^{\gamma d}(\omega)\frac{g}{1-g\Pi^{dd}(\omega)}\Pi^{d\gamma}(\omega). \quad (13)$$

The superscripts of $\Pi(\omega)$ "γ" and "d" indicate the form factors of the vertices of the bubble diagram, which are taken as $\gamma_{\mathbf{k}}^{B_{1g}}$ and $d_{\mathbf{k}}$, respectively. The d-wave form factor comes from the electron-electron interaction which we write as

$$\frac{1}{2}\sum_{\mathbf{k}\mathbf{k}'\sigma\sigma'} g d_{\mathbf{k}} d_{\mathbf{k}'} c^{\dagger}_{\mathbf{k}\sigma} c_{\mathbf{k}\sigma} c^{\dagger}_{\mathbf{k}'\sigma'} c_{\mathbf{k}'\sigma'}, \quad (14)$$

where $g(<0)$ is the coupling strength. This interaction generates the effective interaction shown in Fig. 1(b) and drives the dFSD instability, as was extensively studied theoretically.[1,4,7,8,45] The condition for the instability is given by

$$1 - g\Pi^{dd}(0) = 0. \quad (15)$$

From Eqs. (9) and (11)–(13) we computed the Raman-scattering intensity numerically employing the self-energy shown in Fig. 2.

The selection of diagrams in Fig. 1 corresponds to the lowest-order conserving approximation in the sense of Baym and Kadanoff.[46] The diagrams shown in Fig. 3 in this reference also apply in our case if we consider the dashed line as a sum of the interaction of our Eq. (14) and our boson-mediated, retarded interaction which we have assumed to be independent of momentum. The Hartree terms to the self-energy can be omitted because they are either zero or represent just a renormalization of the chemical potential. The interaction, Eq. (14), does not contribute in the thermodynamic limit to the Fock term of the self-energy in contrast to the boson-mediated interaction which yielded the contribution given in Eq. (7). The vertex is given as the functional derivative of the self-energy with respect to the Green's function. Limiting ourselves to the d-wave vertex we see that it is only the functional derivative of the Hartree term of the interaction, Eq. (14), which contributes to the vertex and produces the chain of bubbles in the d-wave susceptibility. This means that our approximation scheme respects all conservation laws and should be free of artifacts due to an inconsistent approximation.

In the superconducting state the quasiparticle contribution to the Raman-scattering intensity is finite at finite frequencies. Since the self-energies are also much smaller in the superconducting state compared to those in the normal state it seems to be reasonable to neglect self-energy effects in this case.[43] Assuming the following form for the d-wave superconducting gap

$$\Delta_{\mathbf{k}} = \tfrac{1}{2}\Delta_0(\cos k_x - \cos k_y) \quad (16)$$

and the band dispersion, Eq. (2), we obtain for the single bubble diagram [Fig. 1(a) with $\Sigma = 0$],

$$\Pi^{\alpha\beta}(\omega) = \frac{1}{N}\sum_{\mathbf{k}}\alpha_{\mathbf{k}}\beta_{\mathbf{k}}\frac{\Delta_{\mathbf{k}}^2}{E_{\mathbf{k}}^2}\tanh\frac{\beta E_{\mathbf{k}}}{2} \times\left(\frac{1}{\omega-2E_{\mathbf{k}}+i\Gamma}-\frac{1}{\omega+2E_{\mathbf{k}}+i\Gamma}\right), \quad (17)$$

where $E_{\mathbf{k}} = \sqrt{(\epsilon_{\mathbf{k}}-\mu)^2+\Delta_{\mathbf{k}}^2}$. Γ is an infinitesimally small positive quantity which we approximate in our numerical calculations by $\Gamma = 0.001t$. The chemical potential is approximately determined from the relation $\delta = \frac{1}{N}\sum_{\mathbf{k}}\frac{\epsilon_{\mathbf{k}}-\mu}{E_{\mathbf{k}}}\tanh\frac{\beta E_{\mathbf{k}}}{2}$. The Raman-scattering intensity and response function are given again by the formulas (4) and (13), respectively.

B. Raman scattering from phonons

Raman scattering can also determine the spectral function of phonons. Since the interaction driving the dFSD instability couples to phonons with B_{1g} symmetry, we focus on phonons with this symmetry. The corresponding electron-phonon coupling contains the d-wave form factor $d_{\mathbf{k}}$ and is given by

$$g_{\mathbf{k}\mathbf{k}} = g_{\mathrm{ph}} d_{\mathbf{k}}, \quad (18)$$

where $g_{\mathbf{k}\mathbf{k}}$ is the electron-phonon matrix element for the electronic momentum $\mathbf{k}$ and vanishing momentum for the phonon; g_{ph} is the coupling constant. The noninteracting retarded phonon propagator is given by

$$D_0(\omega) = \frac{1}{\omega-\omega_0+i0^+}-\frac{1}{\omega+\omega_0+i0^+}, \quad (19)$$

where ω_0 is the energy of the zero-momentum B_{1g} phonon, which corresponds to $\omega_0 = 4t/15$ ($\approx$40 meV for $t \approx$ 150 meV) in YBCO.[47] The full phonon propagator is given graphically in Fig. 4(a), namely,

$$D^{-1}(\omega) = D_0^{-1}(\omega) - \Sigma_{\mathrm{ph}}(\omega). \quad (20)$$

The free phonon propagator is renormalized by the electron-phonon interaction, which picks up the correlation function of the dFSD instability as shown in Fig. 4(b). The phonon self-energy $\Sigma_{\mathrm{ph}}(\omega)$ [Fig. 4(b)] has exactly the same structure as Fig. 1(a) except for the difference of vertices. The computation of $\Sigma_{\mathrm{ph}}(\omega)$ is straightforward, yielding

$$\Sigma_{\mathrm{ph}}(\omega) = g_{\mathrm{ph}}^2\frac{\Pi^{dd}(\omega)}{1-g\Pi^{dd}(\omega)} \quad (21)$$

$$= g_{\mathrm{ph}}^2\widetilde{\Pi}^{dd}(\omega), \quad (22)$$

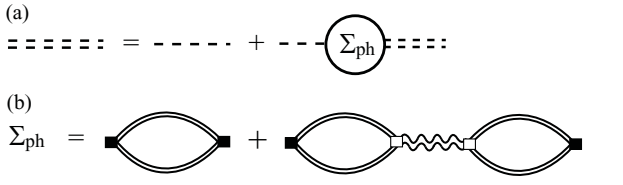

FIG. 4. Graphical representation of the phonon propagator (double dashed line); the single dashed line denotes the noninteracting phonon propagator and the solid square denotes the form factor $g_{\mathrm{ph}}d_{\mathbf{k}}$. The rest of the notation is the same as Fig. 1.

where we have introduced

$$\frac{1}{\widetilde{\Pi}^{dd}(\omega)} = \frac{1}{\Pi^{dd}(\omega)} - g. \tag{23}$$

The quantity $\widetilde{\Pi}^{dd}(\omega)$ would become identical to $\chi^{B_{1g}}(\omega)$ if "γ" were replaced by "d" in Eq. (13). The Raman intensity $S_{\rm ph}$ for phonon scattering becomes

$$S_{\rm ph}(\omega) = -\frac{1}{\pi}[1 + b(\omega)]\mathrm{Im}\, D(\omega), \tag{24}$$

where from Eqs. (20) and (22),

$$\frac{1}{\pi}\mathrm{Im}\, D(\omega) = \frac{4\omega_0^2 g_{\rm ph}^2}{\pi} \frac{\mathrm{Im}\,\widetilde{\Pi}^{dd}(\omega)}{\left[\omega^2 - \omega_0^2 - 2\omega_0 g_{\rm ph}^2\,\mathrm{Re}\,\widetilde{\Pi}^{dd}(\omega)\right]^2 + \left[2\omega_0 g_{\rm ph}^2\,\mathrm{Im}\,\widetilde{\Pi}^{dd}(\omega)\right]^2}. \tag{25}$$

Since $\Pi^{dd}(\omega)$ has already been computed both in the normal and superconducting states in Eqs. (11), (12), and (17), the Raman intensity $S_{\rm ph}(\omega)$ is easily obtained from Eqs. (23)–(25).

1. *Renormalization of the dFSD by the electron-phonon coupling*

It is instructive to provide an expression of the static d-wave charge compressibility,[1,4,8] the susceptibility associated with the dFSD instability. This quantity is obtained by summing up the bubble diagrams connected by electron-electron and electron-phonon interactions as shown graphically in Fig. 5, that is,

$$\kappa_d = -\frac{\Pi^{dd}(0)}{1 - \left[g + g_{\rm ph}^2 D_0(0)\right]\Pi^{dd}(0)} \tag{26}$$

$$= -\frac{\Pi^{dd}(0)}{1 - \tilde{g}\,\Pi^{dd}(0)}, \tag{27}$$

where

$$\tilde{g} = g - \frac{2g_{\rm ph}^2}{\omega_0} \tag{28}$$

is a renormalized coupling constant. Since both $g_{\rm ph}^2$ and ω_0 are positive the original interaction $g(<0)$ is enhanced to become $|\tilde{g}| > |g|$. The coupling to the B_{1g} phonon mode therefore increases the attractive interaction causing the dFSD instability by the amount $\frac{2g_{\rm ph}^2}{\omega_0}$. Therefore the dFSD instability can occur more easily and the instability condition, Eq. (15), is replaced by

$$1 - \tilde{g}\,\Pi^{dd}(0) = 0. \tag{29}$$

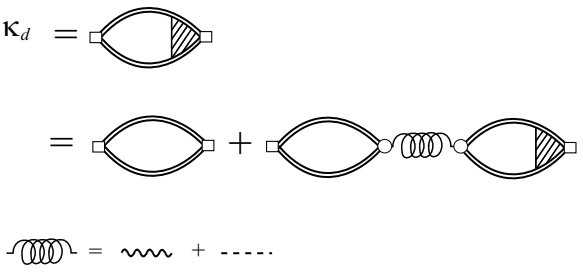

FIG. 5. Graphical representation of the d-wave charge compressibility. A spring denotes two interactions, the electron-electron interaction (wavy line) and the electron-phonon interaction (dashed line), and the corresponding form factors at the vertex (open circle) are $d_{\mathbf{k}}$ and $g_{\rm ph}d_{\mathbf{k}}$, respectively. The shaded vertex is defined by the equality of the first and second line; the rest of the notation is the same as in Fig. 1.

2. *Strength of the electron-phonon coupling*

An estimate for the coupling constant $g_{\rm ph}$ is obtained both from first-principle calculations based on the local-density approximation (LDA) and from experiment. In general, the dimensionless coupling constant λ for a phonon with energy ω_0 and zero momentum is defined by

$$\lambda = 2N(0)\langle|g_{\mathbf{kk}}|^2\rangle_{\rm FS}/\omega_0, \tag{30}$$

where $N(0)$ is the density of states at the Fermi energy for one spin direction, $\langle\cdots\rangle_{\rm FS}$ denotes an average over the Fermi surface, and $g_{\mathbf{kk}}$ is defined by Eq. (18). First-principle LDA calculations yielded for the B_{1g} phonon mode with 40 meV the values $\lambda = 0.02$ (Ref. 48) and 0.06.[49] On the other hand, λ is related to superconductivity-induced self-energy effects of the phonon. It has been argued that the observed self-energy effects are compatible with these values for λ, especially, with the first value.[48] A simple connection between theory and experiment can also be obtained by noting that a phonon well below the superconducting gap at $T = 0$ should show a relative frequency softening of about $\delta\omega_0/\omega_0 = \lambda$.[48] The above 40 meV phonon softens by ~ 1 meV due to superconductivity[50,51] yielding $\lambda \approx 0.02 - 0.03$ in rough agreement with the theoretical prediction.

For a B_{1g} phonon one has $g_{\mathbf{kk}} = g_{\rm ph}d_{\mathbf{k}}$ and $\langle d_{\mathbf{k}}^2\rangle_{\rm FS} = N_d(0)/N(0)$, where $N_d(0)$ is the d-wave projected density at the Fermi energy, namely, $N_d(0) = \int d^2\mathbf{k}\ \delta(\epsilon_{\mathbf{k}} - \mu)d_{\mathbf{k}}^2/(2\pi)^2$. We thus obtain

$$g_{\rm ph}^2 = \frac{\lambda\omega_0}{2N_d(0)}. \tag{31}$$

Since $2N_d(0)$ is equal to the low-energy limit of a single bubble at $T = 0$, namely, $-\Pi^{dd}(0)$, we find $2N_d(0) \sim 1/|g|$, so that $g_{\rm ph}^2 \sim 0.4\lambda t^2$ for $\omega_0 = 4t/15$ and $g = -1.5t$, yielding values between 0.008 and 0.024 for $g_{\rm ph}^2$. In our numerical calculations we use the representative value 0.02.

III. RESULTS

Guided by experiments in YBCO (Refs. 34 and 38) we would like to choose one parameter set in our simple model such that the dFSD instability is reached (a) with decreasing

temperature at around $T \sim t/10$ in the normal state with a doping concentration $\delta = 0.10$ and (b) with decreasing doping at around $\delta \sim 0.20$ for $T \approx 0$. These conditions are approximately fulfilled for $t' = t'' = 0$ and $g = -1.5t$ in our model.[52] For convenience, we use t as the energy unit in presenting our results. Experimentally, the effective t has a value of about 150 meV.

A. Electronic Raman scattering

In the normal state we fix the doping to $\delta = 0.10$ and consider the temperature as a tuning parameter to approach the dFSD instability from high temperatures. For our parameters the dFSD instability occurs at $T = 0.098$. In Fig. 6(a) we show the ω dependence of $\mathrm{Im}\,\chi^{B_{1g}}(\omega)$ for a sequence of temperatures T ranging from 0.10 to 0.20. At high T the weight of $\mathrm{Im}\,\chi^{B1g}(\omega)$ extends very broadly over the whole energy region shown in Fig. 6(a). With decreasing T the low-energy weight ($\omega < 0.2$) gradually increases and sharpens up to form a very steep peak near zero frequency. In Fig. 6(b) we plot the function $S(\omega)$, defined in Eq. (4), which is measured in a Raman-scattering experiment. Although the peak position is not exactly at $\omega = 0$, $S(\omega)$ displays essentially a central peak already well away from the critical temperature. Its spectral weight increases strongly when the critical temperature is approached from above. The energy dependence of $\mathrm{Im}\,\Pi^{dd}(\omega)$ is shown in Fig. 6(c) for several values of T. While $\mathrm{Im}\,\Pi^{dd}(\omega)$ exhibits also a pronounced peak its energy is much larger than that of $\mathrm{Im}\,\chi^{B_{1g}}(\omega)$. Moreover, the effect of temperature is much weaker in $\mathrm{Im}\,\Pi^{dd}(\omega)$ than in $\mathrm{Im}\,\chi^{B_{1g}}(\omega)$. The real part of $\Pi^{dd}(\omega)$ is shown in Fig. 6(d). Its magnitude forms a broad peak at $\omega = 0$ at high temperatures which sharpens up with decreasing temperature. Since the dFSD instability occurs when Eq. (15) is fulfilled, collective fluctuations of the dFSD develop when the magnitude of $\mathrm{Re}\,\Pi^{dd}(0)$ approaches $1/|g| = 2/3$ with decreasing T. Hence the very pronounced peak of $\mathrm{Im}\,\chi^{B_{1g}}(\omega)$ at low energy, seen in Fig. 6(a), is a direct consequence of the development of dFSD correlations.

Next we investigate the evolution of dFSD fluctuations in the superconducting state at $T = 0.001$. Here we take the doping concentration δ as a tuning parameter and approach the dFSD instability by decreasing δ. We choose the superconducting gap amplitude to be $\Delta_0 = t/5$ which seems to be reasonable for cuprate superconductors; the doping dependence of Δ_0 is not important for our conclusions and will not be considered. We obtain $\delta_c = 0.207$ for the critical doping rate where the dFSD instability occurs and consider the region $\delta > \delta_c$. Since there is no qualitative difference between $S(\omega)$ and $\mathrm{Im}\,\chi^{B_{1g}}(\omega)$ we present results only for $S(\omega)$. In Fig. 7(a) we show $S(\omega)$ as a function of ω for several choices of doping; similarly, $\mathrm{Im}\,\Pi^{dd}(\omega)$ and $\mathrm{Re}\,\Pi^{dd}(\omega)$ are presented in Fig. 7(b) at $\delta = 0.25$ and 0.50. At $\delta = 0.50$ the peak position of $S(\omega)$ is nearly the same as that of $\mathrm{Im}\,\Pi^{dd}(\omega)$ because the peak originates from individual excitations. Its position is determined approximately by $\omega = 2|\Delta_{\mathbf{k}}|$ at $\mathbf{k} = \mathbf{k}_F = (k_F, 0)$ or $(0, k_F)$, where k_F is the Fermi momentum along the k_x or k_y direction. With decreasing δ the peak of $S(\omega)$ shifts to lower energies, its half-width decreases, and its height increases strongly. The peak position substantially deviates from that of $\mathrm{Im}\,\Pi^{dd}(\omega)$ [see the results at $\delta = 0.25$ in Figs. 7(a) and 7(b)], indicating the development of collective fluctuations of the dFSD. In fact, the peak position of $S(\omega)$ is near the instability determined by the resonance condition,

$$1 - g\,\mathrm{Re}\,\Pi^{dd}(\omega_{\mathrm{res}}) = 0. \tag{32}$$

The resonance energy ω_{res} is plotted in Fig. 7(c) together with the peak energy of $S(\omega)$ and its peak height. At high δ, Eq. (32)

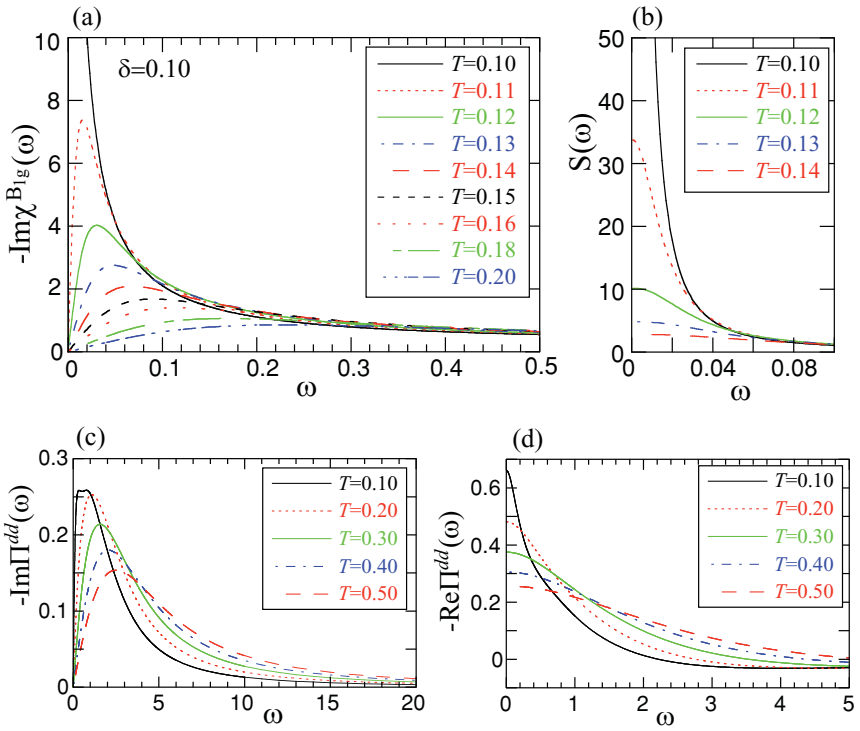

FIG. 6. (Color online) (a) ω dependence of $\mathrm{Im}\,\chi^{B_{1g}}(\omega)$ for a sequence of temperatures T close to the dFSD instability at $T_c = 0.098$ in the normal state at $\delta = 0.10$. (b) Low-energy region of $S(\omega)$ near the dFSD instability. (c) $\mathrm{Im}\,\Pi^{dd}(\omega)$ and (d) $\mathrm{Re}\,\Pi^{dd}(\omega)$ as a function of ω for several values of T.

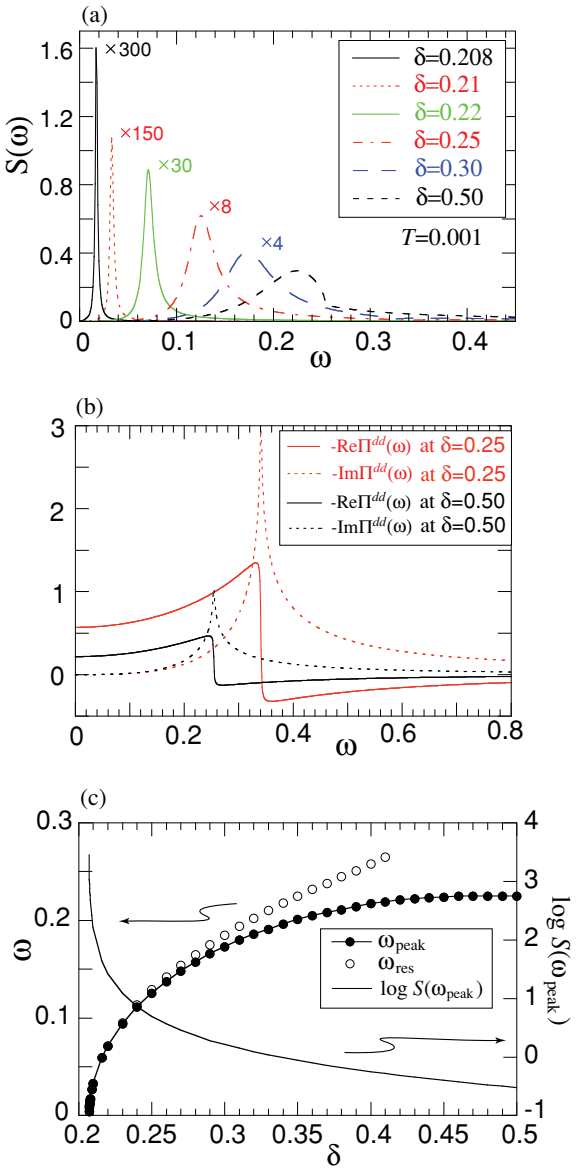

FIG. 7. (Color online) (a) ω dependence of $S(\omega)$ for a sequence of doping concentrations in the superconducting state at $T = 0.001$; the actual value of $S(\omega)$ is obtained by multiplication with the factor indicated near each peak except for $\delta = 0.50$. (b) ω dependence of Re $\Pi^{dd}(\omega)$ (solid line) and Im $\Pi^{dd}(\omega)$ (dashed line) at $\delta = 0.25$ and 0.50. (c) The peak position of $S(\omega)$ (solid circles) and its peak height (solid line) as a function of doping; also shown are the energies $\omega_{\rm res}$ (open circles); the dFSD instability occurs at $\delta_c = 0.207$.

does not have a solution and the peak of $S(\omega)$ must be attributed mainly to individual excitations. For $\delta \lesssim 0.40$, Eq. (32) has a solution. It is seen that upon approaching δ_c, $\omega_{\rm peak}$ becomes almost identical with $\omega_{\rm res}$. Since Im $\Pi^{dd}(\omega) \approx 0$ at $\omega \approx \omega_{\rm res}$ the evolution of $S(\omega)$ in Fig. 7(a) indicates the development of a well-defined collective mode associated with the dFSD. Because of the collective fluctuations the peak intensity of $S(\omega)$ is strongly enhanced upon approaching δ_c and diverges at $\delta = \delta_c$. The peak energy vanishes as $\omega_{\rm peak} \sim (\delta - \delta_c)^{1/2}$, which can be read off from Fig. 7(c).

It is interesting to note the different evolution of $S(\omega)$ in the normal and the superconducting state. In the normal state the magnitude of Re $\Pi^{dd}(\omega)$ has a maximum at $\omega = 0$ and decreases with ω [Fig. 6(d)], whereas in the superconducting state the magnitude of Re $\Pi^{dd}(0)$ corresponds to a local minimum and increases with ω [Fig. 7(b)]. In contrast to the superconducting case the resonance condition, Eq. (32), is not fulfilled in the normal state except at $T = T_c$ and $\omega = 0$. This explains why $S(\omega)$ develops a central peak in the normal state [Fig. 6(a)] and a soft mode in the superconducting state [Fig. 7(a)] and why the width of the peaks is much larger in the normal state than in the superconducting state.

B. Raman scattering from phonons

Raman scattering from B_{1g} phonons exhibits characteristic features near the dFSD instability. As a prominent example we consider the 40 meV phonon in YBCO (Ref. 47) which has in an approximate tetragonal classification, where the chains are neglected, B_{1g} symmetry. Our parameter values become $\omega_0 = 4/15$ and $g_{\rm ph}^2 = 0.02$, as discussed in Sec. II B.

Figure 8(a) shows $S_{\rm ph}(\omega)$ in the normal state for $\delta = 0.10$ and several values for T. In the presence of the electron-phonon interaction the critical temperature occurs at $T_c = 0.126$ which is higher than in the case without electron-phonon interaction. Well above this temperature, for instance, at $T = 0.20$ $S_{\rm ph}(\omega)$ consists of one single peak at $\omega \approx \omega_0$ representing a usual quasiharmonic phonon. The peak position moves only slightly upward and its spectral weight decreases somewhat with decreasing temperature. However, at low frequencies dramatic changes occur: approaching T_c from high temperatures a central peak develops. It extends over a rather broad energy region $\omega \lesssim 0.1$, but nearer to the instability its half-width decreases and its spectral weight increases strongly. It is caused by the coupling of the phonon to dFSD fluctuations. The occurrence of a double peak in the phonon spectral function can be understood by studying the denominator of the phonon spectral function, Eq. (25), omitting Im $\widetilde{\Pi}^{dd}(\omega)$,

$$\mathrm{Res}(\omega) = \omega^2 - \omega_0^2 - 2\omega_0 g_{\rm ph}^2\, \mathrm{Re}\, \widetilde{\Pi}^{dd}(\omega). \qquad (33)$$

As shown in Fig. 8(b), Re $\widetilde{\Pi}^{dd}(\omega)$ decreases monotonically with frequency and becomes small around $\omega \approx \omega_0$. Because $g_{\rm ph}^2 = 0.02$ is also small Res(ω) becomes zero at $\omega \approx \omega_0$ giving rise to the quasiharmonic phonon mode. Since the magnitude of Re $\widetilde{\Pi}^{dd}(\omega)$ assumes its maximum at $\omega = 0$ and increases there with decreasing T, it eventually reaches the value $\omega_0/(2g_{\rm ph}^2)$ so that Res(ω) becomes zero also at $\omega = 0$. This situation occurs just at T_c, because the expression Re $\widetilde{\Pi}^{dd}(0) = -\omega_0/(2g_{\rm ph}^2)$ reduces to Re $\Pi^{dd}(0) = 1/\tilde{g}$ via Eq. (23) which corresponds to the onset of the dFSD instability [Eq. (29)]. Hence both Res(ω) and Im $\widetilde{\Pi}^{dd}(\omega)$ for $\omega \approx 0$ are very small near T_c which causes a central peak close to the dFSD instability. The long tail in frequency of the central peak reflects the fact that the magnitudes of Res(ω) and Im $\widetilde{\Pi}^{dd}(\omega)$ only slowly increase with increasing ω. In Fig. 8(c) we plotted the peak positions and peak heights of the phonon spectral function as a function of T. The lower peak position is denoted by $\omega_s^{\rm ph}$. We see that the central peak emerges well above $T_c = 0.126$ and rapidly acquires a large spectral weight with decreasing T which diverges at $T = T_c$. The high-frequency part of the phonon spectral function does not show a pronounced temperature dependence

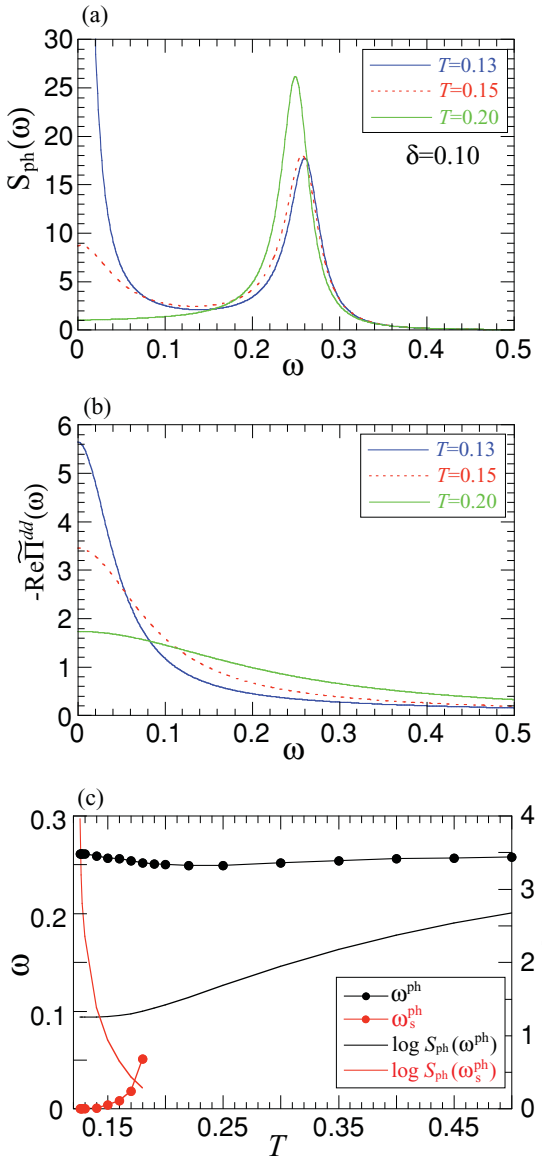

FIG. 8. (Color online) ω dependence of S_{ph} (a) and $\mathrm{Re}\,\widetilde{\Pi}^{dd}(\omega)$ (b) for several choices of temperatures in the normal state at $\delta = 0.10$; the renormalized critical temperature of the dFSD instability is $T_c = 0.126$. (c) Peak positions ω^{ph} and $\omega_s^{\mathrm{ph}} (< \omega^{\mathrm{ph}})$ of $S_{\mathrm{ph}}(\omega)$ and their peak heights as a function of T.

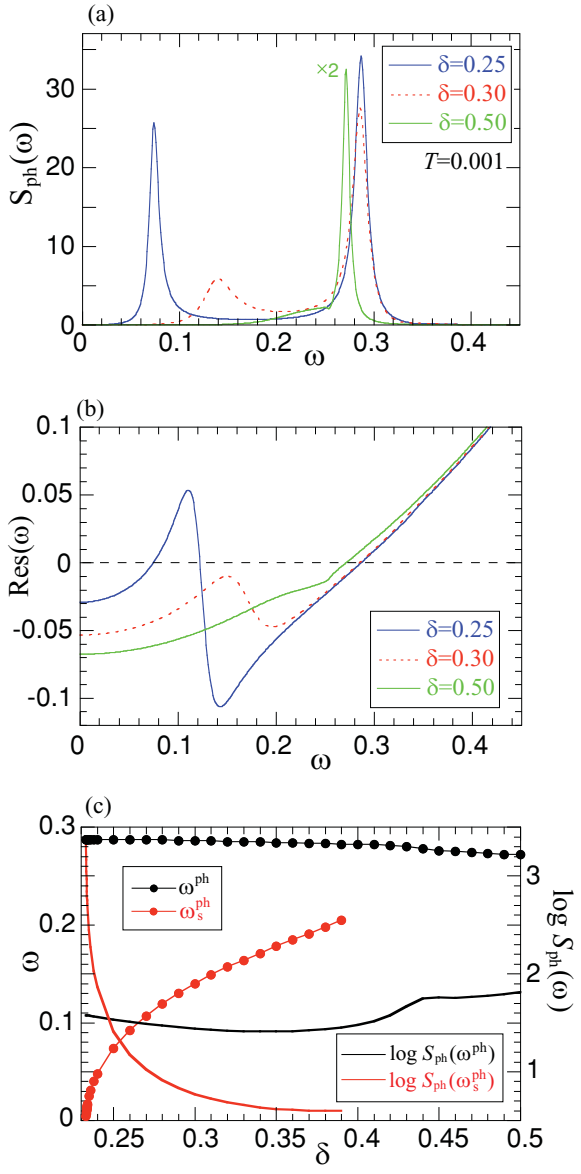

FIG. 9. (Color online) (a) ω dependence of $S_{\mathrm{ph}}(\omega)$ for several choices of δ in the superconducting state at $T = 0.001$; the actual value at $\delta = 0.50$ is obtained by multiplying with a factor of 2. (b) ω dependence of $\mathrm{Res}(\omega)$ for different δ. (c) Peak positions ω^{ph} and $\omega_s^{\mathrm{ph}} (< \omega^{\mathrm{ph}})$ of $S_{\mathrm{ph}}(\omega)$ as a function of δ together with their peak heights. The dFSD instability occurs at $\delta_c = 0.233$.

despite the proximity to the dFSD instability. The peak intensity near $\omega = \omega_0$ is suppressed at lower T because of the increase of the magnitude of $\mathrm{Im}\,\widetilde{\Pi}^{dd}(\omega)$ around $\omega \approx \omega_0$ upon approaching T_c.

The phonon spectral function in the superconducting state is shown in Fig. 9(a) for several doping concentrations. At $\delta = 0.50$ the spectral function shows a quasiharmonic phonon with one sharp peak at $\omega \fallingdotseq \omega_1 \approx \omega_0$, where $\mathrm{Res}(\omega_1) = 0$ [Eq. (33) and Fig. 9(b)]. With decreasing δ the position of this peak shifts only slightly to higher energies but is essentially unchanged. At $\delta = 0.30$ an additional broad peak emerges at the low energy $\omega \approx 0.14$ in Fig. 9(a). Its position is approximately given by the energy at which $\mathrm{Res}(\omega)$ forms a local maximum [see Fig. 9(b)]. Decreasing δ further to 0.25 the lower peak becomes sharper, moves to lower energies, and its spectral weight increases. The equation $\mathrm{Res}(\omega) = 0$ now has three solutions, ω_1, ω_2, and ω_3 [see Fig. 9(b)], with $\omega_1 > \omega_2 > \omega_3 \geqslant 0$. The solution $\omega_1 \approx \omega_0$ yields the sharp high-frequency peak in $S_{\mathrm{ph}}(\omega)$, while the solution ω_3 is responsible for the low-frequency peak. The solution of ω_2 cannot produce a peak in $S_{\mathrm{ph}}(\omega)$ because $\mathrm{Im}\,\widetilde{\Pi}^{dd}(\omega)$ has a peak near the energy ω_2 and thus broadens out any structure in this frequency region. These three solutions exist until ω_3 becomes zero. At this point the dFSD instability occurs which follows from a similar argument as given below Eq. (33). In Fig. 9(c) we present the peak positions of $S_{\mathrm{ph}}(\omega)$ and their heights as a function of δ. The high-frequency peak in the phonon spectral function, appearing around $\omega \approx \omega_0 = 4/15$, displays only a very weak doping dependence in spite of the

proximity to the dFSD instability. Its height also depends only weakly on δ on a logarithmic scale. The coupling of the phonon to collective fluctuations of the dFSD leads to the appearance of a second peak at low energy which softens in frequency and increases in intensity upon approaching the dFSD instability. The lower peak energy vanishes as $\sim(\delta-\delta_c)^{1/2}$ and its intensity diverges when approaching the critical doping $\delta_c = 0.233$. The emergent low-energy peak is a well-defined collective mode driven by fluctuations of the dFSD in the sense that the resonance condition $\mathrm{Res}(\omega) \approx 0$ as well as $\mathrm{Im}\,\widetilde{\Pi}^{dd}(\omega) \approx 0$ is fulfilled at the peak energy.

It is intriguing to realize that the original quasiharmonic B_{1g} phonon mode does not behave like a soft phonon when the dFSD instability is approached. Instead the phonon spectral function splits into a high-frequency part which is practically unaffected by the instability and an emergent low-frequency part which behaves like a soft and a central mode in the superconducting and normal state, respectively. This double-peak structure in the spectral function is robust if the original phonon energy ω_0 is sufficiently large. Otherwise, the phonon peak in the normal state may overlap with the emergent low-energy structure broadening the double-peak structure into a seemingly single peak. In the superconducting state ω_0 should be chosen to be larger than the peak energy in $\mathrm{Im}\,\widetilde{\Pi}^{dd}(\omega)$, which is approximately given by the peak position of $S(\omega)$ shown in Fig. 7(a). Otherwise, the original phonon mode softens down to zero energy upon approaching the dFSD instability and no additional low-energy peak emerges, in contrast to Fig. 9(a).

IV. DISCUSSION AND CONCLUSION

We have studied Raman scattering in a system where the interaction between electrons drives the system toward a dFSD instability, both in the normal and superconducting states. The electrons are assumed to live on a square lattice with hopping amplitudes t, t', and t'' between first, second, and third nearest neighbors. The interaction is a charge-density interaction with internal d-wave symmetry and interaction strength g. The parameters t', t'', and g are set up to mimic the strong tendency toward the dFSD instability in YBCO. One could wonder whether our choice of $t' = t'' = 0$ and $g = -1.5t$ is unrealistic because the presence of substantial second- and third-nearest-neighbor hoppings is well known in cuprates[53] and the value of g simply seems too big. We would like to stress that the above parameter values should be interpreted as effective parameters within a phenomenological approach.[52] It is worth mentioning that a mean-field dFSD instability occurs in the t-J model with realistic parameters t', t'', and $g(=-3J/8)$ for cuprates at lower carrier densities at temperatures as high as $0.2J$.[1] However, it is not easy to perform the above calculations directly for the t-J model. Nevertheless, we believe that the essential features of such a more microscopic approach are retained at least qualitatively in our simple phenomenological treatment.

One result of our calculation is that the spectral function of a B_{1g} phonon exhibits a double-peak structure when the dFSD instability is approached as shown in Figs. 8 and 9. The double-peak structure might seem similar to the emergence of a central peak near structural phase transitions for several perovskites such as $SrTiO_3$,[54,55] $LaAlO_3$,[56] and $KMnF_3$.[57] However, the quasiharmonic phonon also exhibits softening for these materials, in contrast to our results. Moreover, the central mode in the experiments has been explained in terms of impurity scattering,[58] a different mechanism from ours. The double-peak structure we have obtained in Figs. 8 and 9 can be interpreted as a general aspect in a coupled system of phonons and order-parameter fluctuations. In fact, similar results to ours were obtained in a different context, for example, in pseudospin-phonon systems[59] and in superconductors with a strong electron-phonon coupling[60,61] explaining the double peaks of Raman spectrum with E_{2g} symmetry observed in MgB_2.[62]

For YBCO a strong tendency toward xy symmetry breaking was observed.[31,32,34,38] Its order parameter may be defined by

$$\phi = \frac{1}{2}\sum_{\sigma}\langle c^{\dagger}_{i+x\sigma}c_{i\sigma} + c^{\dagger}_{i\sigma}c_{i+x\sigma}\rangle - \langle c^{\dagger}_{i+y\sigma}c_{i\sigma} + c^{\dagger}_{i\sigma}c_{i+y\sigma}\rangle \tag{34}$$

$$= \frac{1}{N}\sum_{\mathbf{k}\sigma} d_{\mathbf{k}}\langle c^{\dagger}_{\mathbf{k}\sigma}c_{\mathbf{k}\sigma}\rangle, \tag{35}$$

where i denotes the site on a square lattice and we have assumed that ϕ is constant. Equations (34) or (35) is nothing but the order parameter of a dFSD instability.[1,4,8] It is characterized by Ising symmetry and thus two solutions, $\phi = \phi_0$ and $-\phi_0$, are degenerate. In order to favor either solution, it may be natural to apply a small external perturbation which breaks xy symmetry in the CuO_2 plane. In fact, the compound YBCO contains the CuO chains, which serves as a uniaxial strain. In this case, the dFSD instability becomes a crossover phenomenon, but the crossover is still sharp as far as the external anisotropy is weak, which seems to hold in YBCO.

From the very strong anisotropy of the magnetic excitation spectrum in $YBCO_{6.45}$,[34] the presence of an underlying quantum critical point (QCP) has been conjectured in the doping range $\delta \approx 8$–$10\,\%$.[35,36] This conjecture could be tested in a rather direct way using Raman scattering in the superconducting state (see Figs. 7 and 9). The measurement of the Nernst coefficient by Daou *et al.*[38] determined the doping dependence of the dFSD instability in the region of 11–18% doping and suggested that the pseudogap temperature T^* corresponds to the onset of the dFSD instability. Raman scattering can directly measure dFSD fluctuations and instabilities generated by them (see Figs. 6 and 8), and thus prove the consistency of transport and light-scattering data. Moreover, the resistivity measurement by Daou *et al.*[63] suggested that T^* goes down to zero in the overdoped region, implying the presence of a QCP associated with the dFSD instability inside the superconducting state. Theory[35,36] and transport measurements,[38,63] however, conjecture quite different values for the position of the QCP as a function of doping which also could be clarified by Raman scattering in the superconducting state (see Figs. 7 and 9). The neutron-scattering experiments for $YBCO_{6.45}$,[34] $YBCO_{6.6}$,[31,32] and $YBCO_{6.85}$ (Ref. 31) suggested a delicate interplay between the tendency toward a dFSD and the singlet pairing formation in agreement with theory.[33,37] Raman scattering around T_c or the pseudogap temperature T^* can directly reveal how the dFSD competes with the singlet pairing at different doping levels. Available Raman-scattering

data[64] for YBCO with 10% carrier doping do not suggest the strong enhancement of the low-energy spectral weight, seen in Fig. 6, but the data were obtained only at a few temperatures. More detailed experimental studies including doping dependence are worth performing.

The La-based cuprate superconductors were extensively discussed in terms of the charge-stripe order.[65] However, the scenario based on the dFSD instability was also proposed.[1,66,67] Although the authors of Refs. 64 and 68 interpreted the B_{1g} Raman-scattering spectra for La-based cuprates with 10% in terms of charge stripes, their data exhibit a spectrum very similar to Fig. 6(a), indicating direct evidence of the development of dFSD correlations. The data in Refs. 64 and 68 are worth reconsidering.

The dFSD is a generic feature in correlated electron systems and occurs in the t-J (Refs. 1–3) and Hubbard[4,5,69,70] models, in systems where electrons interact via a central force,[71,72] and quite generally in Fermi liquids with a van Hove saddle point.[73] Therefore the dFSD instability can be expected to occur in a variety of materials. In order to apply the present theory in the normal state we had to include self-energy effects. While quantitative features of the Raman spectrum certainly depend on details of the self-energy, it is not unreasonable to assume that its qualitative features associated with the proximity of the dFSD instability are rather robust. In this sense we hope that our results will serve to analyze Raman-scattering data for various materials, which possibly lie close to a dFSD instability. In particular, compelling but indirect evidence for a dFSD instability has accumulated in Sr327 both experimentally[10–12] and theoretically.[17–25] It would be desirable to also perform Raman-scattering measurements in this system to confirm the dFSD instability in a more direct and decisive way.

In summary, we have studied Raman scattering from electrons and phonons in the normal and superconducting state near a dFSD instability. In the normal state the inclusion of the electronic self-energy is vital for which we have used experimental input from ARPES data in high-T_c cuprates.[41,42] Approaching the dFSD instability from the normal state a central peak emerges both in electronic scattering and in the spectral function of a phonon with B_{1g} symmetry. Approaching the dFSD instability in the superconducting state by decreasing doping concentrations a sharp soft mode appears in electronic Raman scattering. This soft mode also appears in the spectral function of the phonon as an additional low-energy feature, whereas the usual phonon peak is nearly unaffected by the proximity of the instability. Our study was motivated by recent transport measurements[38] which suggest a dFSD instability in a wide doping region in YBCO. Since Raman scattering measures directly the correlation function of order-parameter fluctuations associated with the dFSD instability, such measurements, together with our theoretical curves, could confirm in a rather direct way the dFSD in real systems.

ACKNOWLEDGMENTS

We would like to thank M. Bakr and B. Keimer for valuable discussions and W. Metzner for a critical reading of the manuscript. H.Y. appreciates the warm hospitality of Max-Planck-Institute for Solid State Research and acknowledges support by a Grant-in-Aid for Scientific Research from Monkasho.

[1] H. Yamase and H. Kohno, J. Phys. Soc. Jpn. **69**, 332 (2000); **69**, 2151 (2000).
[2] A. Miyanaga and H. Yamase, Phys. Rev. B **73**, 174513 (2006).
[3] B. Edegger, V. N. Muthukumar, and C. Gros, Phys. Rev. B **74**, 165109 (2006).
[4] C. J. Halboth and W. Metzner, Phys. Rev. Lett. **85**, 5162 (2000).
[5] B. Valenzuela and M. A. H. Vozmediano, Phys. Rev. B **63**, 153103 (2001).
[6] I. J. Pomeranchuk, Sov. Phys. JETP **8**, 361 (1959).
[7] H.-Y. Kee, E. H. Kim, and C.-H. Chung, Phys. Rev. B **68**, 245109 (2003); I. Khavkine, C.-H. Chung, V. Oganesyan, and H.-Y. Kee, *ibid*. **70**, 155110 (2004).
[8] H. Yamase, V. Oganesyan, and W. Metzner, Phys. Rev. B **72**, 035114 (2005).
[9] S. A. Kivelson, E. Fradkin, and V. J. Emery, Nature (London) **393**, 550 (1998).
[10] S. A. Grigera, P. Gegenwart, R. A. Borzi, F. Weickert, A. J. Schofield, R. S. Perry, T. Tayama, T. Sakakibara, Y. Maeno, A. G. Green, and A. P. Mackenzie, Science **306**, 1154 (2004).
[11] R. A. Borzi, S. A. Grigera, J. Farrell, R. S. Perry, S. J. S. Lister, S. L. Lee, D. A. Tennant, Y. Maeno, and A. P. Mackenzie, Science **315**, 214 (2007).
[12] A. W. Rost, R. S. Perry, J.-F. Mercure, A. P. Mackenzie, and S. A. Grigera, Science **325**, 1360 (2009).
[13] A. Tamai, M. P. Allan, J. F. Mercure, W. Meevasana, R. Dunkel, D. H. Lu, R. S. Perry, A. P. Mackenzie, D. J. Singh, Z.-X. Shen, and F. Baumberger, Phys. Rev. Lett. **101**, 026407 (2008).
[14] R. S. Perry, K. Kitagawa, S. A. Grigera, R. A. Borzi, A. P. Mackenzie, K. Ishida, and Y. Maeno, Phys. Rev. Lett. **92**, 166602 (2004).
[15] R. A. Borzi, S. A. Grigera, R. S. Perry, N. Kikugawa, K. Kitagawa, Y. Maeno, and A. P. Mackenzie, Phys. Rev. Lett. **92**, 216403 (2004).
[16] J.-F. Mercure, S. K. Goh, E. C. T. O'Farrell, R. S. Perry, M. L. Sutherland, A. Rost, S. A. Grigera, R. A. Borzi, P. Gegenwart, and A. P. Mackenzie, Phys. Rev. Lett. **203**, 176401 (2009).
[17] H.-Y. Kee and Y. B. Kim, Phys. Rev. B **71**, 184402 (2005).
[18] H. Doh, Y. B. Kim, and K. H. Ahn, Phys. Rev. Lett. **98**, 126407 (2007).
[19] H. Yamase and A. A. Katanin, J. Phys. Soc. Jpn. **76**, 073706 (2007).
[20] H. Yamase, Phys. Rev. B **76**, 155117 (2007).
[21] C. Puetter, H. Doh, and H.-Y. Kee, Phys. Rev. B **76**, 235112 (2007).
[22] H. Yamase, Phys. Rev. B **80**, 115102 (2009).
[23] A. F. Ho and A. J. Schofield, Europhys. Lett. **84**, 27007 (2008).
[24] M. H. Fischer and M. Sigrist, Phys. Rev. B **81**, 064435 (2010).
[25] C. Puetter, J. G. Rau, and H.-Y. Kee, Phys. Rev. B **81**, 081105(R) (2010).
[26] H. Doh and H.-Y. Kee, Phys. Rev. B **75**, 233102 (2007).
[27] H. Adachi and M. Sigrist, Phys. Rev. B **80**, 155123 (2009).

[28]H. Yamase and P. Jakubczyk, Phys. Rev. B **82**, 155119 (2010).
[29]S. Raghu, A. Paramekanti, E-.A. Kim, R. A. Borzi, S. A. Grigera, A. P. Mackenzie, and S. A. Kivelson, Phys. Rev. B **79**, 214402 (2009).
[30]W.-C. Lee and C. Wu, Phys. Rev. B **80**, 104438 (2009).
[31]V. Hinkov, S. Pailhès, P. Bourges, Y. Sidis, A. Ivanov, A. Kulakov, C. T. Lin, D. Chen, C. Bernhard, and B. Keimer, Nature (London) **430**, 650 (2004).
[32]V. Hinkov, P. Bourges, S. Pailhès, Y. Sidis, A. Ivanov, C. D. Frost, T. G. Perring, C. T. Lin, D. P. Chen, and B. Keimer, Nat. Phys. **3**, 780 (2007).
[33]H. Yamase and W. Metzner, Phys. Rev. B **73**, 214517 (2006).
[34]V. Hinkov, D. Haug, B. Fauqué, P. Bourges, Y. Sidis, A. Ivanov, C. Bernhard, C. T. Lin, and B. Keimer, Science **319**, 597 (2008).
[35]E.-A. Kim, M. J. Lawler, P. Oreto, S. Sachdev, E. Fradkin, and S. A. Kivelson, Phys. Rev. B **77**, 184514 (2008).
[36]Y. Huh and S. Sachdev, Phys. Rev. B **78**, 064512 (2008).
[37]H. Yamase, Phys. Rev. B **79**, 052501 (2009).
[38]R. Daou, J. Chang, D. LeBoeuf, O. Cyr-Choinière, F. Laliberté, N. Doiron-Leyraud, B. J. Ramshaw, R. Liang, D. A. Bonn, W. H. Hardy, and L. Taillefer, Nature **463**, 519 (2010).
[39]A. Hackl and M. Vojta, Phys. Rev. B **80**, 220514(R) (2009).
[40]D. J. Singh and I. I. Mazin, e-print arXiv:1007.0255.
[41]P. D. Johnson, T. Valla, A. V. Fedorov, Z. Yusof, B. O. Wells, Q. Li, A. R. Moodenbaugh, G. D. Gu, N. Koshizuka, C. Kendziora, S. Jian, and D. G. Hinks, Phys. Rev. Lett. **87**, 177007 (2001).
[42]L. Zhao, J. Wang, J. Shi, W. Zhang, H. Liu, J. Meng, G. Liu, X. Dong, W. Lu, G. Wang, Y. Zhu, X. Wang, Q. Peng, Z. Wang, S. Zhang, F. Yang, C. Chen, Z. Xu, and X. J. Zhou, e-print arXiv:1002.0120.
[43]T. P. Devereaux and R. Hackl, Rev. Mod. Phys. **79**, 175 (2007).
[44]G. D. Mahan, *Many-Particle Physics* (Plenum, New York, 1990).
[45]C. A. Lamas, D. C. Cabra, and N. Grandi, Phys. Rev. B **78**, 115104 (2008).
[46]G. Baym and L. P. Kadanoff, Phys. Rev. **124**, 287 (1961).
[47]L. Pintschovius, Phys. Status Solidi B **242**, 30 (2005).
[48]C. Thomsen, M. Cardona, B. Friedl, C. O. Rodriguez, I. I. Mazin, and O. K. Andersen, Solid State Commun. **75**, 219 (1990).
[49]K.-P. Bohnen, R. Heid, and M. Krauss, Europhys. Lett. **64**, 104 (2003).
[50]M. Krantz, H. J. Rosen, R. M. Macfarlane, and V. Y. Lee, Phys. Rev. B **38**, 4992 (1988).
[51]M. Bakr, A. P. Schnyder, L. Klam, D. Manske, C. T. Lin, B. Keimer, M. Cardona, and C. Ulrich, Phys. Rev. B **80**, 064505 (2009).
[52]We performed the same calculations for (i) $t' = -t/6$, $t'' = 0$, and $g = 1.2t$ and (ii) $t' = -0.30t$, $t'' = 0.15t$, and $g = 1.5t$, and confirmed the same conclusions.
[53]T. Tohyama and S. Maekawa, Supercond. Sci. Technol. **13**, R17 (2000).
[54]T. Riste, E. J. Samuelsen, K. Otnes, and J. Feder, Solid State Commun. **9**, 1455 (1971).
[55]S. M. Shapiro, J. D. Axe, G. Shirane, and T. Riste, Phys. Rev. B **6**, 4332 (1972).
[56]J. K. Kjems, G. Shirane, K. A. Müller, and H. J. Scheel, Phys. Rev. B **8**, 1119 (1973).
[57]K. Gesi, J. D. Axe, G. Shirane, and A. Linz, Phys. Rev. B **5**, 1933 (1972).
[58]B. I. Halperin and C. M. Varma, Phys. Rev. B **14**, 4030 (1976).
[59]Y. Yamada, H. Takatera, and D. L. Huber, J. Phys. Soc. Jpn. **36**, 641 (1974).
[60]R. Zeyher and G. Zwicknagl, Z. Phys. B **78**, 175 (1990).
[61]R. Zeyher, Phys. Rev. Lett. **90**, 107002 (2003).
[62]J. W. Quilty, S. Lee, A. Yamamoto, and S. Tajima, Phys. Rev. Lett. **88**, 087001 (2002).
[63]R. Daou, N. Doiron-Leyraud, D. LeBoeuf, S. Y. Li, F. Laliberté, O. Cyr-Choinière, Y. J. Jo, L. Balicas, J.-Q. Yan, J.-S. Zhou, J. B. Goodenough, and L. Taillefer, Nat. Phys. **5**, 31 (2009).
[64]L. Tassini, F. Venturini, Q.-M. Zhang, R. Hackl, N. Kikugawa, and T. Fujita, Phys. Rev. Lett. **95**, 117002 (2005).
[65]S. A. Kivelson, I. P. Bindloss, E. Fradkin, V. Oganesyan, J. M. Tranquada, A. Kapitulnik, and C. Howald, Rev. Mod. Phys. **75**, 1201 (2003).
[66]H. Yamase and H. Kohno, J. Phys. Soc. Jpn. **70**, 2733 (2001).
[67]H. Yamase, Phys. Rev. B **75**, 014514 (2007).
[68]F. Venturini, Q.-M. Zhang, R. Hackl, A. Lucarelli, S. Lupi, M. Ortolani, P. Calvani, N. Kikugawa, and T. Fujita, Phys. Rev. B **66**, 060502(R) (2002).
[69]I. Grote, E. Körding, and F. Wegner, J. Low Temp. Phys. **126**, 1385 (2002); V. Hankevych, I. Grote, and F. Wegner, Phys. Rev. B **66**, 094516 (2002).
[70]A. Neumayr and W. Metzner, Phys. Rev. B **67**, 035112 (2003).
[71]J. Quintanilla and A. J. Schofield, Phys. Rev. B **74**, 115126 (2006).
[72]J. Quintanilla, M. Haque, and A. J. Schofield, Phys. Rev. B **78**, 035131 (2008).
[73]M. V. Zverev, J. W. Clark, Z. Nussinov, and V. A. Khodel, Phys. Rev. B **82**, 125111 (2010).